Available online at www.sciencedirect.com
ScienceDirect
Journal of the European Ceramic Society 27 (2007) 2255–2263
www.elsevier.com/locate/jeurceramsoc

Strontium barium niobate-relating structural developments and dielectric constant

P.K. Patro [a,1], R. Khatirkar [a], I. Samajdar [a], A.R. Kulkarni [a,*], C.S. Harendranath [b]

[a] *Department of Metallurgical Engineering and Materials Science, Indian Institute of Technology Bombay, Powai, Mumbai 400076, India*
[b] *Sophisticated Analytical Instrument Facility (SAIF), Indian Institute of Technology Bombay, Powai, Mumbai 400076, India*

Received 22 May 2006; received in revised form 3 August 2006; accepted 10 August 2006
Available online 25 September 2006

Abstract

Strontium barium niobate (SBN) ceramics, synthesized through partial co-precipitation, was sintered at—6, 12 and 24 h, respectively, at 1250, 1300 and 1350 °C. Structural developments, developments in porosity, grain size, residual stress and crystallographic texture and its effect on dielectric constants were studied at different sintering conditions. The bulk crystallographic texture was largely unaffected by the sintering conditions used, though all other structural parameters evolved through sintering schedule. An effort was made to relate the changes in dielectric constant with the changes in structural parameters. Normal grain growth or changes in residual stress pattern either had relatively insignificant effects on dielectric constant or decoupling the relative effects was difficult from the present set of data. On the other hand, the strongest increase in dielectric constant was achieved through reduced porosity/defects, while abnormal growth caused the largest drop.

Keywords: Porosity; Grain boundary; (Sr,Ba)Nb_2O_6; Texture; Residual Stress

1. Introduction

Strontium barium niobate (SBN), a tetragonal tungsten bronze (TTB) structured ferroelectric material, has received considerable attention as a lead-free electroceramic with wide applicability—electro-optic, photo-refractive, SAW, piezoelectric and pyroelectric.[1–8] Since SBN ($Sr_{1-x}Ba_xNb_2O_6$), exists in the ferroelectric phase for a wide composition range ($x = 0.25$–0.75), it is possible to obtain tailor made material with desired property and operational temperature range through optimized composition.[9] Present day applications of SBN are largely limited to single crystals.[10–12] Even though considerable progress has been made in the growth of high quality SBN single crystals,[13] applications are restricted mainly due to cost-economics.

SBN can typically be synthesized in polycrystalline form by solid-state reaction synthesis,[14–16] from sol–gel route,[17] hydrolysis aging,[18] partial coprecipitation,[19] coprecipitation,[20] combustion[21] and from EDTA complex chemical route.[22] However, none of the synthesis approaches for polycrystalline material has been successful in bringing the ferroelectric/piezoelectric values close to that of single crystal. Secondary processing, sintering and associated grain growth, may, however, offer possibilities of property improvements through optimized structural development. Controlled abnormal grain growth, for example, has been used quite successfully in obtaining absolute control of crystallographic texture and hence magnetic properties in transformer steel.[23–25] If a similar approach is conceivable in SBN or the limits of a secondary processing like sintering in pursuing an optimized structure property relation are not really known. To explore this was the broad objective of the present study.

In a polycrystalline ferroelectric material, the dielectric property is affected by number of factors—porosity/defect, grain size, crystallographic texture and residual stress. Elimination of porosity/defects (and an increase in density) is expected to improve dielectric constant,[26,27] while presence of compressive residual stress is often considered to be beneficial.[28,29] On the other hand, dielectric constant is expected to increase and then decrease with increase in grain size.[30,31] Existence of large grain size, grain size being much larger than the domain size,

* Corresponding author. Tel.: +91 22 2576 7636; fax: +91 22 2572 3480.
E-mail address: ajit.kulkarni@iitb.ac.in (A.R. Kulkarni).
[1] Present address: Energy Conversion Materials Section, Materials Group, Bhabha Atomic Research Centre, Vashi Complex, New Mumbai 400705, India.

0955-2219/$ – see front matter © 2006 Elsevier Ltd. All rights reserved.
doi:10.1016/j.jeurceramsoc.2006.08.011

however, may not restrict applications—as appropriate mechanical or laser scribing[23] may be used effectively for domain refining. Since ferroelectric materials are associated with an axis of easy polarization, it is expected to have higher dielectric constant, when measured in this direction.[32] In other words, the crystallographic orientation in the polycrystalline materials plays a key role on the dielectric and ferroelectric property of the material.[33] It is, however, important to point out that though the role of the individual structural parameters is relatively well charted, their relative or combined effects in a polycrystalline material can be more complicated and definitely less understood.

SBN50 used in the present case was synthesized by partial coprecipitation method and was sintered at different temperature–time combinations. The synthesis and developments in dielectric constant with sintering was described in a previous study.[19] The present study reports the structural developments during sintering and makes an attempt to relate the changes in dielectric constant with the structural developments.

2. Experimental

The synthesis of SBN50 by partial coprecipitation, microstructural studies by SEM, measurements of density and dielectric property are described in a previous study.[19] As mentioned in the previous study the partially coprecipitated powder was calcined at 1200 °C to obtain single phase of SBN50. Further, this single phase powder was sintered at 1250, 1300 and 1350 °C for 6, 12 and 24 h, respectively. During the sintering process the heating and cooling rate was maintained at 3 °C/min. A brief microstructural description is also discussed in this paper. The present study involved detailed characterization of residual stress, bulk crystallographic texture and the microtexture; and these are described in the present section. PANalytical X'pert MRD system was used for measurements of bulk crystallographic texture and residual stress. In the absence of single crystal stiffness constant data for SBN50 (X-ray elastic constants), the values of the slope of d (interplanar distance) versus $\sin^2\Psi$ are taken as indicative of stress. For bulk crystallographic texture measurement, four incomplete pole figures were measured. X-ray ODFs (orientation distribution functions) were calculated from the pole figures using a commercial ODF program–Labosoft, which uses the ADC algorithm.[34] Microtexture measurements were obtained on the samples polished through diamond and colloidal silica, the latter involving simultaneous etch-polish action. The samples were gold coated (10–20 nm thick) and then analyzed by OIM (Orientation Imaging Microscopy)—using a commercial TSL system on a FEI Quanta 200 HV SEM.

3. Results

3.1. Microstructural study

The microstructural studies of the sintered pellets were carried out using a CAMECA SU30 scanning electron microscope in the SE mode. Fig. 1(a)–(i), are the respective micrographs at the sintering temperature of 1250, 1300 and 1350 °C for 6, 12 and 24 h each. A considerable amount of porosity is observed for 1250 °C for 6 h with the grain size varying from 2 to 8 μm. The micrograph also reflects that the sintering stage is at its initial stage because of presence of neck formation in between the grains. A relatively better compacted microstructure is observed for the sintering condition of 1250 °C for 12 h and 1250 °C for 24 h with grain size varying between 7–15 and 10–15 μm, respectively. For 1300 °C for 6 h, with average grain size of 8 μm. On close observation, presence of some residual pores can also be observed in this micrograph. Except for the marginal improvement in average grain size (10 μm) in 1300 °C for 12 h, there is not much difference in microstructure in comparison to 1300 °C for 6 h. However, the residual surface pores are absent in this case. For 1300 °C for 24 h, more number of elongated grains with tetragonal morphology can be seen having some grains higher than 30 μm. For 1350 °C for 6 h, the average grain size increased to 10 μm. For 1350 °C for 12 h and 1350 °C for 24 h the presence of some large grains can be seen. These are having uniaxial grain growth (>50 μm) and can be termed as abnormality in the grain growth.

Here, the effect of these uniaxial elongated grains on the dielectric properties is of our interest and wish to correlate with texture/microtexture and observation of residual stress in the material.

3.2. Dielectric constant and density measurements

The variation of dielectric constant with temperature for SBN50 sintered at different time–temperature combinations is summarized in Fig. 2. As shown in the figure, three distinct trends were observed for the respective sintering temperatures. At 1250 °C a steady increase (from 574 to 1283) in dielectric constant with increase in sintering time was observed, while at 1350 °C a steady drop (from 1406 to 968) was noted. At 1300 °C, however, the dielectric constant was not affected noticeably (remaining nearly at ≈1100) by the sintering time. The rationale for changes in the dielectric property should exist in the structural developments, developments in crystallographic texture, relative density, microstructure and/or stresses; and these were systematically characterized. The results from density measurements are included in this section, while other structural characterizations are elaborated in the next sections.

The variation of experimentally measured density with temperature for different sintering combinations is given in Fig. 3. As shown in Fig. 3, there was a noticeable increase in density from 4.18 to 4.93 g/cm^3 with increase in sintering time (from 6 to 12 h) at 1250 °C. The density, however, did not change significantly between 12 and 24 h. A steady, though less significant, decrease in density (from 4.94 to 4.62 g/cm^3) was observed for sintering at 1350 °C; while at 1300 °C the density was more or less constant at 4.95 g/cm^3. It is to be noted that the theoretical density of the SBN50 is 5.42 g/cm^3 and the lower values of experimental densities indicate presence of porosities.

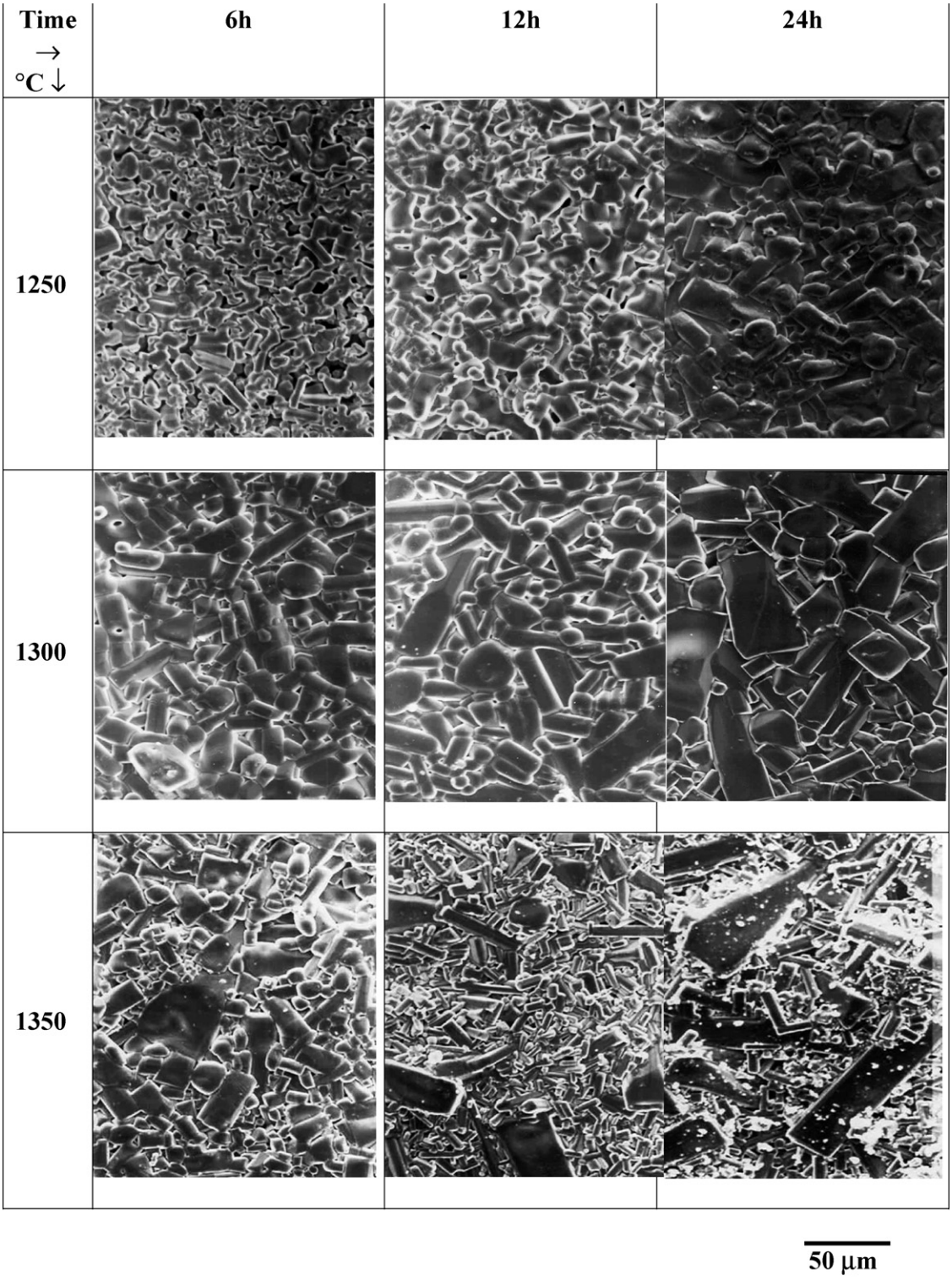

Fig. 1. Scanning electron micrograph of SBN50 sintered at different temperatures and durations.

3.3. Observations on residual stress

As discussed in Section 2, estimation of exact values of residual stress would involve a database on at least the elastic modulus and the Poisson's ratio values, which are difficult to estimate in a typical electro-ceramics. The peak-shifts, the index of elastic residual stress, have been measured at different ψ (0 to ±45) and the data were plotted as d versus $\sin^2\psi$ plots. The slopes of such plots are included in Fig. 4. It is to be noted that a negative and positive slope, respectively, stand for compressive and tensile stresses, while the numerical values are an estimate of the amount of the stress. Stresses after 6 h sintering at all sintering temperatures were compressive (see Fig. 4). The trends of stress developments

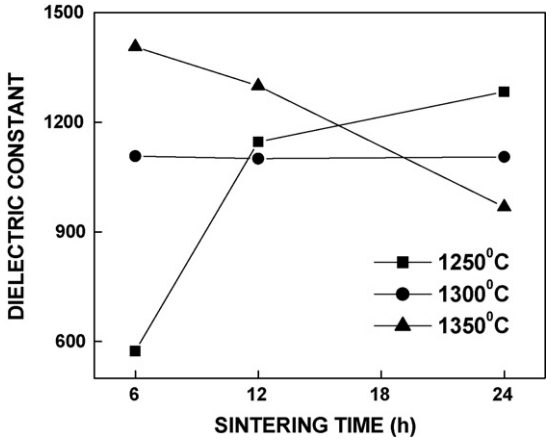

Fig. 2. Variation of dielectric constant with sintering time for different sintering temperatures.

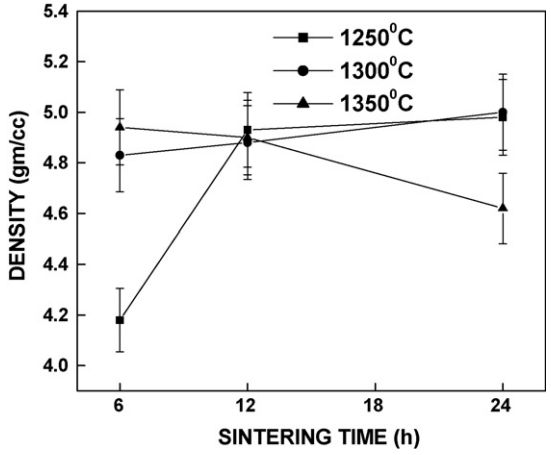

Fig. 3. Variation of density (experimental—with error bars indicating scatter in experimental data) with sintering time for different sintering temperatures.

were, however, different subsequently. At 1250 °C the compressive stress increased, while at 1350 °C it decreased. At 1300 °C the compressive stress first increased and then decreased significantly.

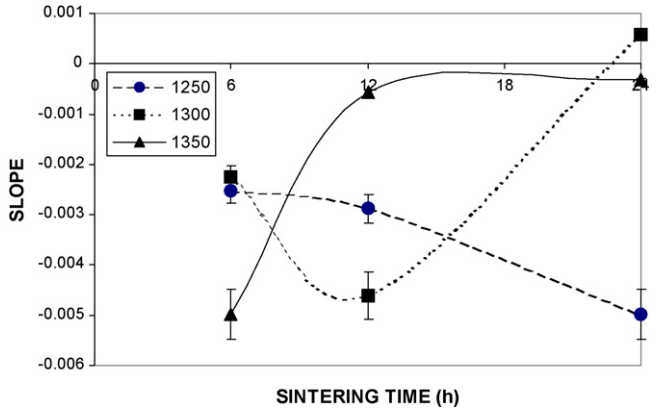

Fig. 4. Slopes of d vs. $\sin^2 \Psi$ plots for different sintering conditions. The positive and negative values represent, respectively, the tensile and compressive residual stresses, while the numerical values are expected to scale with the stress magnitude.

Table 1
Maximum ODF intensity and the average intensity of the (3 3 4) fiber, the strongest fiber present, are given for different sintering conditions

Sample	Maximum ODF intensity	{3 3 4} fiber intensity
1250 °C for 6 h	14.2	7.0
1250 °C for 12 h	10.7	7.2
1250 °C for 24 h	11.7	7.4
1300 °C for 6 h	10.5	7.0
1300 °C for 12 h	16.0	6.8
1300 °C for 24 h	11.3	6.9
1350 °C for 6 h	11.6	7.0
1350 °C for 12 h	9.7	6.8
1350 °C for 24 h	12	7.5

3.4. Bulk crystallographic texture

As the sintering process can be considered as an axisymmetric process, inverse pole figures (IPFs) were used to represent developments in bulk crystallographic texture with respect to sintering conditions (see Fig. 5). Table 1 summarizes the maximum ODF intensity values and average intensity values for (3 3 4) fiber, strongest fiber present. As shown in the IPFs, as in Fig. 5, the crystallographic texture did not change qualitatively with sintering conditions. Though there were changes in the extent of texturing (as given by the ODF maximum intensity values, Table 1), the strongest fiber present (3 3 4) did not change noticeably, see Table 1. As ⟨0 0 1⟩ is the axis of easy polarization for SBN,[32,33] changes in ⟨0 0 1⟩ fiber were also monitored. It is important to point out that the average intensity (remaining around 2) or volume fraction of the ⟨0 0 1⟩ fiber did not show any significant changes with sintering conditions. In other words, though changes in relative texturing were observed, bulk crystallographic texture (including presence of ⟨0 0 1⟩ fiber) was otherwise unaffected by the sintering conditions.

3.5. Orientation imaging microscopy

Orientation imaging microscopy (OIM) is finding increasing applications in electro-ceramics,[35] largely because of its ability to bring the orientation effects in a mesoscopic structure. In the present study, OIM was considered necessary to bring out exact grain sizes and also to provide trends in grain size distributions and distributions in low angle grain boundary (LAGB) concentrations at different sintering conditions. Fig. 6 shows the OIMs (representative areas—as the total area covered at each sintering stage was at least 1 mm × 1 mm) and Fig. 7 provides grain size distributions. The relative concentrations of LAGBs are given in Table 2. It is to be noted that 1250 °C for 6 h sintered sample did not give indexable Kikuchis, possible because of large concentration of defects (including porosities) present.

As shown in Figs. 6 and 7, sintering at 1350 °C led to the so-called abnormal grain growth.[23] Though the mechanisms of normal and abnormal grain growth are considered[36] to be the same, appearance of 'visible' abnormal growth (1350 °C for 12 h) led to a noticeable drop in LAGB. Normal grain growth, on the other hand, was associated with an increase in LAGB concentration. The grain sizes distribution, in general, and abnormal

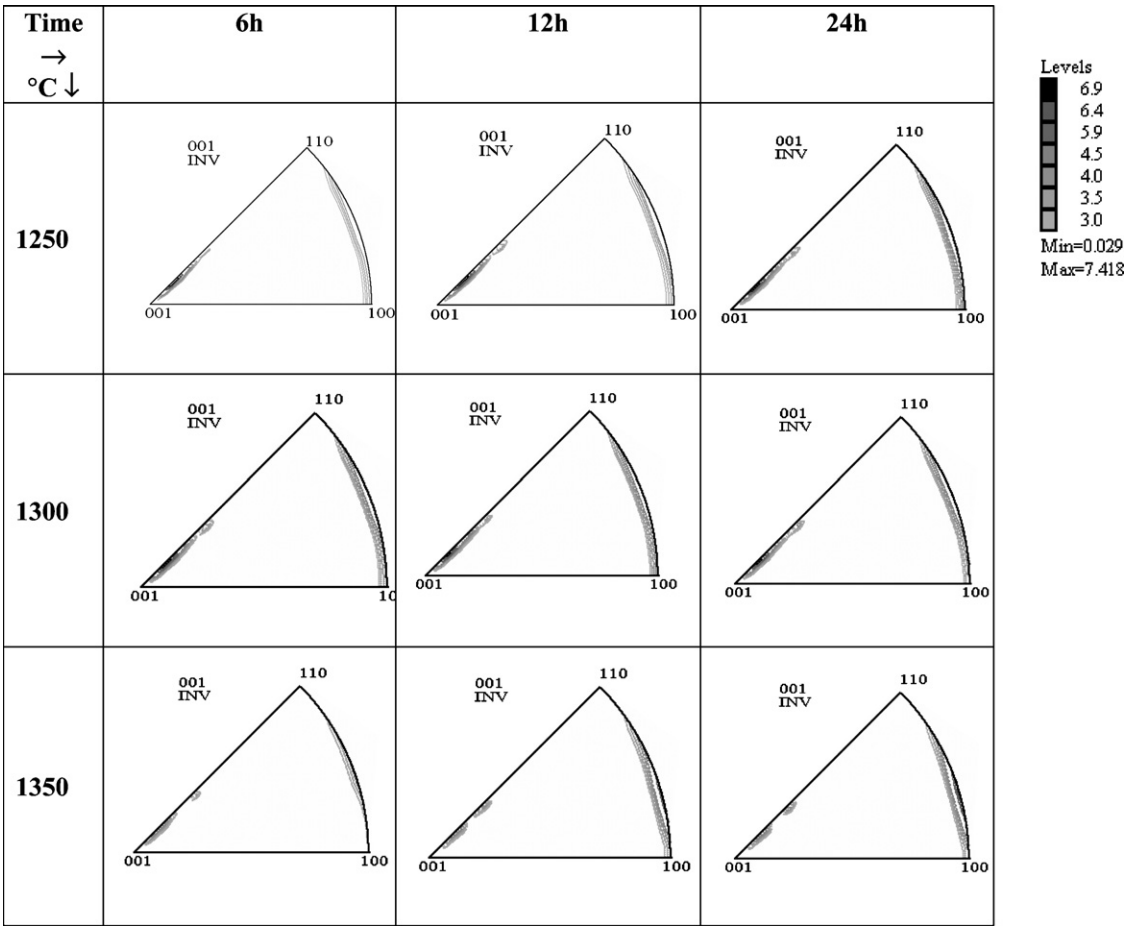

Fig. 5. Inverse pole figures (IPF) obtained for different sintering conditions. The contour levels used for the IPFs are indicated.

grain growth, in particular, had a strong effect on the dielectric constant—subject of the subsequent discussion, Section 4.

It is clear from the micrographs and OIM images (see Figs. 1 and 6) that the AGG appeared at 1350 °C. The signature of AGG is growth of few grains, while majority of the grains actually do shrink. Samples undergoing 1300 °C sintering, on the other hand, showed normal grain growth. It needs to be pointed out that the mechanism(s) of both normal and abnormal grain growth are the same[24]—the differences in microstructural evolution is caused by relative growth advantage for selected few or by growth disadvantage for the majority. It is clear that 1350 °C sintering could bring such advantage or disadvantage, though exact rationale (normally AGG is caused by differences in grain boundary pinning—either orientation pinning or pinning through second phase[24]) behind that remains unresolved.

4. Discussion

It is well known that the dielectric constant depends on structural parameters—crystallographic texture,[32,33,36] residual stress,[28,29] porosity/defects[26,27] and grain size distribution.[37] Decoupling all these factors is difficult theoretically. The present set of experimental results may provide some hints at such decoupling. Before doing so, it is necessary to highlight the

Table 2
Orientation imaging microscopy (OIM) estimated low angle grain boundary concentrations at different sintering conditions

	1–5°	5–10°	10–15°	15–20°	Total
1250 °C for 6 h	–	–	–	–	–
1250 °C for 12 h	0.135675	0.009341	0.056116	0.056991	0.258123
1250 °C for 24 h	0.174731	0.008217	0.062789	0.064919	0.310656
1300 °C for 6 h	0.141096	0.007409	0.039707	0.037813	0.226025
1300 °C for 12 h	0.174767	0.006423	0.068617	0.081316	0.331123
1300 °C for 24 h	0.21862	0.009698	0.061409	0.065345	0.355072
1350 °C for 6 h	0.129574	0.007136	0.069986	0.055283	0.261979
1350 °C for 12 h	0.116639	0.007672	0.013575	0.010441	0.148327
1350 °C for 24 h	0.187503	0.008256	0.007204	0.015081	0.218044

It is to be noted that 0–1° boundaries were considered within the experimental tolerance of the OIM measurements.

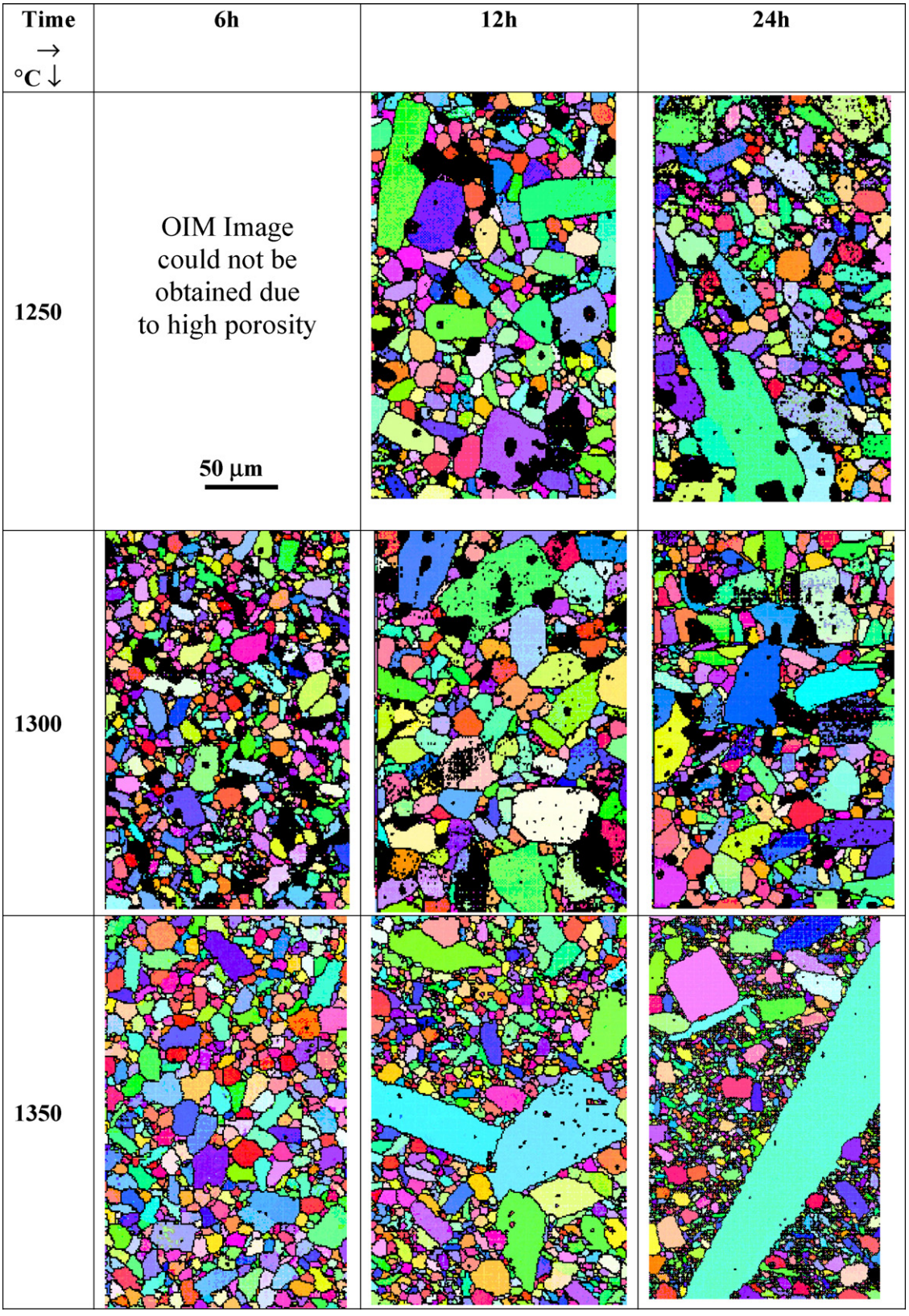

Fig. 6. Orientation imaging microscopy (OIM) images for SBN50 at different sintering conditions. Boundaries of more than 20° are marked along with the black patches indicating porosities.

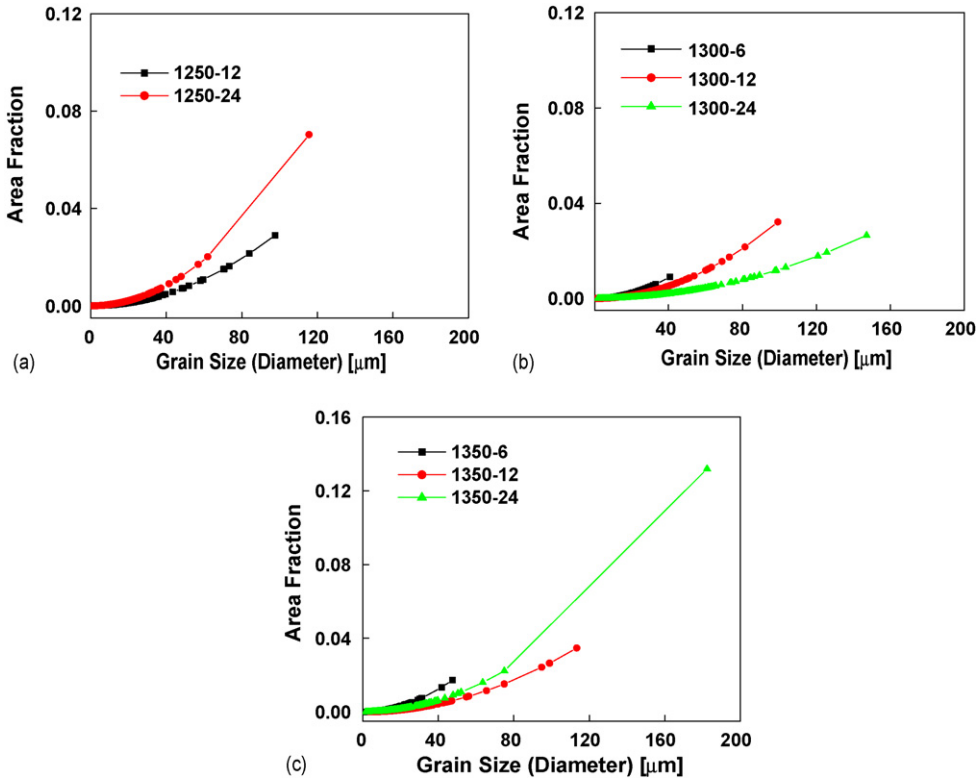

Fig. 7. Grain size distributions for sintering at (a) 1250 °C, (b) 1300 °C and (c) 1350 °C. The distributions were obtained from scans of at least 1 mm × 1 mm area.

dielectric constant changes along with the estimated changes in structural parameters. This is given in Table 3. It is important to point out, as indicated earlier in Section 3.3, that changes in bulk crystallographic texture were insignificant and hence are not listed in Table 3. The density, an effective measure for porosity, increased substantially between 6 and 12 h sintering at 1250 °C. At all other sintering conditions, however, the estimated density changes did fall within the scatter of experimental data.

Changes in dielectric constant at three sintering temperatures can be related to the changes in structural parameter and a comparison is summarized below (also given in details in Table 3):

- 1250 °C: Substantial increase in dielectric constant between 6 and 12 h sintering was clearly related to reduced porosity/defects.[26,b] Between 12 and 24 h the increase in dielectric constant was relatively less significant, an increase possibly associated with both increase in grain size and compressive residual stress.
- 1300 °C: Almost no change in dielectric constant for both time intervals was estimated, though a monotonic increase in grain size (through normal grain growth) and small increase followed by a substantial drop in compressive residual stresses were observed. It is possible that changes in grain size distribution and compressive residual stress had counterbalancing effects. Decoupling their relative contributions is rather impossible from this set of data points.
- 1350 °C: A slight drop in dielectric constant between 6 and 12 h was followed by a substantial decrease between 12 and 24 h. Though compressive residual stress dropped signifi-

Table 3
Changes in dielectric constant (ε), experimental density (ρ in g/cm^3), slope of d vs. $\sin^2\Psi$ (indicating residual stress changes, as in Fig. 4) and average grain size d (as in Fig. 7) between two time intervals (6–12 and 12–24 h) at three different sintering temperatures

Sintering temperature	Sintering time	
	6–12 h	12–24 h
1250 °C		
ε	*572*	*137*
ρ	*0.75*	0.05
S	−0.00036	−0.00211
d	–	1.48
1300 °C		
ε	−7	5
ρ	0.05	0.12
S	−0.00235	0.005198
d	19.75	15.25
1350 °C		
ε	*−107*	*−331*
ρ	−0.04	−0.28
S	0.004411	0.000241
d	17.6 (abnormal grain growth)	18.1 (abnormal grain growth)

Significant changes, in dielectric constant and in structural parameters, are given in 'italics'. Initiation of noticeable abnormal grain growth is also indicated.

[b] Possible role of grain size changes could not be indexed.

cantly in the first stage, it remained nearly the same at the second stage of time interval. The substantial drop in dielectric constant is clearly related to shifting grain size and grain size distribution caused by the abnormal grain growth.

To summarize, the present set of results do highlight clearly the role of two structural parameters on the dielectric constant. Elimination of porosity and defects led to substantial increase in dielectric constant (1250 °C), while substantial abnormal grain growth led to a significant drop in dielectric constant (1350 °C). The role of compressive residual stress, at least in the range of stresses observed, seems to be relatively minor.

5. Conclusions

Based on the results and discussion above, following conclusions have been drawn:

- The crystallographic texture did not change noticeably with sintering conditions.
- Effects of normal grain growth and residual stress pattern on the dielectric constant could not be established convincingly from the present set of experimental data.
- In the range of sintering conditions used, elimination of porosity/defects seems to have the strongest effect on the increase in dielectric constant.
- Significant abnormal grain growth (and associated shift in grain size distributions) decreased the dielectric constant significantly.

Acknowledgements

The authors acknowledge DST 'National Facility for OIM and Texture', Dept. of Met. Engg. and Materials Sc. IIT-Bombay and Electron Microscopy Facility of SAIF, IIT-Bombay. One of the authors (P.K. Patro), acknowledge Council of Scientific and Industrial Research, India for Senior Research Fellowship grant.

References

1. Trubelja, M. P., Ryba, E. and Smith, D. K., A study of positional disorder in strontium barium niobate. *J. Mater. Sci.*, 1996, **31**, 1435–1443.
2. Heartling, G. H. and Land, C. E., Hot pressed (Pb,La)(Zr,Ti)O_3 ferroelectric ceramic for electro-optic applications. *J. Am. Ceram. Soc.*, 1971, **54**, 1–11.
3. Antisigin, V. D., Kotsov, E. G., Malinovsky, V. K. and Sterelyukhina, L. N., Electrooptics of thin ferroelectric films. *Ferroelectrics*, 1981, **38**, 761–763.
4. Neurgaonkar, R. R., Oliver, R. and Cory, W. K., Piezoelectricity in tungsten bronze crystals. *Ferroelectrics*, 1994, **160**, 265–276.
5. Neurgaonkar, R. R. and Cross, L. E., Piezoelectric tungsten bronze crystals for SAW device applications. *Mater. Res. Bull.*, 1986, **21**, 893–899.
6. Glass, A. M., Investigation of electrical properties of $Sr_{1-x}Ba_xNb_2O_6$ with special reference to pyroelectric detection. *J. Appl. Phys.*, 1969, **40**, 4699–4713.
7. Ewbank, M. D., Neurgaonkar, R. R., Cory, W. K. and Feinberg, J., Photorefractrive properties of strontium barium niobate. *J. Appl. Phys.*, 1987, **62**, 374–380.
8. Rytz, D., Wechsler, B. A., Schwartz, R. N., Nelson, C. C., Brandle, C. D., Valentino, A. J. *et al.*, Temperature dependence of photorefractive properties of strontium barium niobate ($Sr_{0.6}Ba_{0.4}Nb_2O_6$). *J. Appl. Phys.*, 1989, **66**, 1920–1924.
9. Vandamme, N. S., Sutherland, A. E., Jones, L., Bridger, K. and Winzer, S. R., Fabrication of optically transparent and electrooptic strontium barium niobate ceramics. *J. Am. Ceram. Soc.*, 1994, **74**, 1785–1792.
10. Neurgaonkar, R. R., Kalisher, M. H., Lim, T. C., Staples, E. J. and Keester, K. L., Czochralski single crystal growth of strontium barium niobate ($Sr_{.61}Ba_{.39}Nb_2O_6$) for surface acoustic wave applications. *Mater. Res. Bull.*, 1980, **15**, 1235–1240.
11. Sugiyama, Y., Yagi, S., Yokohama, I. and Hatakeyama, I., Holographic recording in cerium doped strontium barium niobate *a*-axis single crystal fibers. *Jpn. J. Appl. Phys.*, 1992, **31**, 708–712.
12. Yamamoto, J. K., McHenry, D. A. and Bhalla, A. S., Strontium barium niobate single-crystal fibers: optical and electro-optic properties. *J. Appl. Phys.*, 1991, **70**, 3215–3222.
13. Lee, H. S. K., Bridgman growth and characterization of single crystals of strontium barium niobate and related materials. *Diss. Abstr. Int. B*, 2000, **61**, 1032–1033.
14. Patro, P. K., Kulkarni, A. R. and Harendranath, C. S., Dielectric and ferroelectric behavior of SBN50 synthesized by solid-state route using different precursors. *Ceram. Int.*, 2004, **30**, 1405–1409.
15. Fang, T., Wu, N. and Shiau, F., Formation mechanism of strontium barium niobate ceramic powders. *J. Mater. Sci. Lett.*, 1994, **13**, 1746–1748.
16. Deshpande, S. B., Potdar, H. S., Godbole, P. D. and Date, S. K., Preparation and ferroelectric properties of SBN:50 ceramics. *J. Am. Ceram. Soc.*, 1992, **75**, 2581–2585.
17. Hirano, S., Yogo, T., Kikuta, K. and Ogiso, K., Preparation of strontium barium niobate by sol–gel method. *J. Am. Ceram. Soc.*, 1992, **75**, 1697–1700.
18. Lu, S. G., Mak, C. L. and Wong, K. H., Low temperature preparation and size effect of strontium barium niobate ultra fine powder. *J. Am. Ceram. Soc.*, 2001, **84**, 79–84.
19. Patro, P. K., Kulkarni, A. R. and Harendranath, C. S., Microstructure and dielectric properties of strontium barium niobate ceramic, synthesized using partial coprecipitation. *J. Eur. Ceram. Soc.*, 2003, **23**, 1329–1335.
20. Patro, P. K., Kulkarni, A. R. and Harendranath, C. S., Combustion synthesis of $Sr_{0.5}Ba_{0.5}Nb_2O_6$ and effect of fuel on its microstructure and dielectric properties. *Mater. Res. Bull.*, 2003, **38**, 249–259.
21. Patro, P. K., Deshmukh, R. D., Kulkarni, A. R. and Harendranath, C. S., Synthesis of $Sr_{0.5}Ba_{0.5}Nb_2O_6$ by coprecipitation method—dielectric and microstructural characteristics. *J. Electroceram.*, 2004, **13**, 479–485.
22. Panda, A. B., Pathak, A. and Pramanik, P., Low temperature preparation of nanocrystalline solid solution of strontium-barium-niobate by chemical process. *Mater. Lett.*, 2002, **52**, 180–186.
23. Matsuo, M., Texture control in the production of grain oriented silicon steels. *ISI J. Int.*, 1989, **29**, 809–827.
24. Humphreys, F. J. and Hatherly, M., *Recrystallization and related annealing phenomena*. Elsevier Science, UK, 1995.
25. Takahashi, N. and Harase, J., Recent development of technology of grain oriented silicon steel. *Mater. Sci. Forum.*, 1996, **204–206**, 143–154.
26. Sumirat, I., Ando, Y. and Shimamura, S., Theory of dielectric constant in porous materials. *Trans. Mater. Res. Soc. Jpn.*, 2004, **29**, 1089–1092.
27. Okazaki, K. and Igarashi, H., Importance of microstructure in electronic ceramics. In *Ceram. Microstruct., Proc. Int. Mater. Symp.*, ed. R. M. Fulrath and J. A. Pask, 1977, pp. 564–583.
28. Kimura, T., Miyamoto, S. and Yamaguchi, T., Microstructure development and dielectric properties of potassium strontium niobate ceramics. *J. Am. Ceram. Soc.*, 1990, **73**, 127–130.
29. Vij, J. K., Pressure, temperature and frequency dependence of the dielectric properties of strontium barium niobate. *Phys. Status Solidi A*, 1982, **74**, 225–232.
30. Palkar, V. R. and Purandare, S. C., Finite size effects in ferroelectric oxides. *Ferroelectr. Rev.*, 2000, **2**, 169–215.
31. Zhao, Z., Buscaglia, V., Viviani, M., Buscaglia, M. T., Mitoseriu, L., Testino, A. *et al.*, Grain-size effects on the ferroelectric behavior of dense nanocrystalline $BaTiO_3$ ceramics. *Phys. Rev. B*, 2004, **70**, 024107–024115.
32. Duran, C., Trolier-McKinstry, S. and Messing, G. L., Fabrication and electrical properties of textured $Sr_{0.53}Ba_{0.47}Nb_2O_6$ ceramics by templated grain growth. *J. Am. Ceram. Soc.*, 2000, **83**, 2203–2213.
33. Duran, C., Trolier-McKinstry, S. and Messing, G. L., Dielectric and piezoelectric properties of textured $Sr_{0.53}Ba_{0.47}Nb_2O_6$ ceramics pre-

pared by templated grain growth. *J. Mater. Res.*, 2002, **17**, 2399–2409.
34. Pawlik, K., Determination of the orientation distribution function from pole figures in arbitrarily defined cells. *Phys. Stat. Sol. (B)*, 1986, **134**, 477–483.
35. Abbruzzese, G. and Lücke, K., A theory of texture controlled grain growth. I. Derivation and general discussion of the model. *Acta Metall.*, 1986, **34**, 905–914.
36. Messing, G. L., Trolier-McKinstry, S., Sabolsky, E. M., Duran, C., Kwon, S., Brahmaroutu, B. *et al.*, Templated grain growth of textured piezoelectric ceramics. *Crit. Rev. Solid State Mater. Sci.*, 2004, **29**, 45–96.
37. Jimenez, B., Alemany, C. and Mendiola, J., Phase transitions in ferroelectric ceramics of the type $Sr_{0.5}Ba_{0.5}Nb_2O_6$. *J. Phys. Chem. Solids*, 1985, **46**, 1383–1386.